Polyhedron 157 (2019) 225–231

Contents lists available at ScienceDirect

Polyhedron

journal homepage: www.elsevier.com/locate/poly

Photochemical deposition, characterization and optical properties of thin films of ThO_2

Y. Huentupil [a], G. Cabello-Guzmán [b], B. Chornik [c], R. Arancibia [d], G.E. Buono-Core [a,*]

[a] Instituto de Química, Pontificia Universidad Católica de Valparaíso, Valparaíso, Chile
[b] Departamento de Ciencias Básicas, Facultad de Ciencias, Universidad del Bío-Bío, Chillán, Chile
[c] Departamento de Física, Facultad de Ciencias Físicas y Matemáticas, Universidad de Chile, Casilla 487-3, Santiago 8370415, Chile
[d] Departamento de Química Analítica e Inorgánica, Universidad de Concepción, Concepción, Chile

ARTICLE INFO

Article history:
Received 25 May 2018
Accepted 8 October 2018
Available online 13 October 2018

Keywords:
Thorium dioxide
Thin film
Photochemical deposition
Luminescent sensing
CO sensor

ABSTRACT

Thorium oxide thin films were successfully prepared by direct UV irradiation of amorphous films composed of thorium(IV) β-diketonate precursor complexes on Si(100) and quartz substrates. The ThO_2 films were characterized by X-ray photoelectron spectroscopy (XPS), X-ray diffraction (XRD) and atomic force microscopy (AFM). The X-ray diffraction patterns showed that the films that annealed at T° below 550 °C were amorphous. The films that annealed at 550 °C and above exhibited a preferred orientation along the (111) plane. Both the as-photodeposited and annealed ThO_2 films exhibited a good optical quality with transparency in the visible region better than 85%. Photoluminescence of ThO_2 thin films was reversibly quenched when exposed to 60 ppm of CO at room temperature.

1. Introduction

Thorium oxide (ThO_2) is an actinide that is characterized as a white powder with a fluorite structure. Thorium dioxide has a face centered cubic (fluorite) crystal structure. The metal ion is in the center of a cube, the corner positions of which are occupied by 8 oxygen anions. This cationic cubic site has a center of symmetry and is stable, inert because and highly resistant to corrosion [1]. Thorium oxide has high resistivity and is a good thermic conductor. In nature, thorium oxide is found in many minerals, the most common of which torianita (70% ThO_2), also known as thoria, is the most reflective oxide known and the most chemically stable oxide ceramic, with a single stable +4 oxidation state and melting temperature of approximately 3000 °C [2]. This oxide has been investigated because of its interesting properties, such as its luminescence and reflective properties [3–7]. In addition, because its low angle reflectance is twice as high as that of standard materials, thin films of thoria have been investigated for use as reflectors for extreme ultraviolet (EUV) and soft X-rays [8–10].

Thorium oxide thin films have been prepared by different methods, such as spray-pyrolysis [11,12], physical vapor deposition (PVD) [13], sol–gel techniques [14], radio-frequency magnetron sputtering [8] and argon-sputtering [15]. ThO_2 films have been used in a variety of applications, such as catalysts [16], gas sensors [17] and electrodes [18,19]. Recently, both hydrothermal and thermal treatments of thorium complexes with the amino acid asparagine were used to prepare thorium dioxide crystalline powders [20]. Photochemically induced synthesis of nanocrystalline ThO_2 from aqueous solutions containing thorium nitrate and ammonium formate has also been reported [21].

In our previous works, we have reported the synthesis of a variety of metal oxide thin films [22–28] using a photochemical method for deposition. This method, known as PMOD (photochemical metal–organic deposition), uses metal–organic complexes as precursors, which are deposited as amorphous films on substrates by a spin coating technique. The precursor films are then irradiated with ultraviolet light, causing photoextrusion of the ligands and leaving a thin film of the metallic oxide on the surface. We found that the suitable precursors for this method were β-diketonate metal complexes with alkyl or aryl substituents in the ligand. We therefore propose β-diketonate Th(IV) complexes as precursors for the photochemical deposition of thorium oxide thin films (Scheme 1).

Here, we report the preparation and characterization of ThO_2 thin films by direct photochemical deposition using Th(IV)diketonate complexes as source materials. The potential use of these films as luminescent gas sensors is also reported. Although electrical measurements are more frequently used in gas sensing applications, this study will try to delimit the potential of luminescence as

* Corresponding author.
E-mail address: gonzalo.buonocore@pucv.cl (G.E. Buono-Core).

https://doi.org/10.1016/j.poly.2018.10.023
0277-5387/

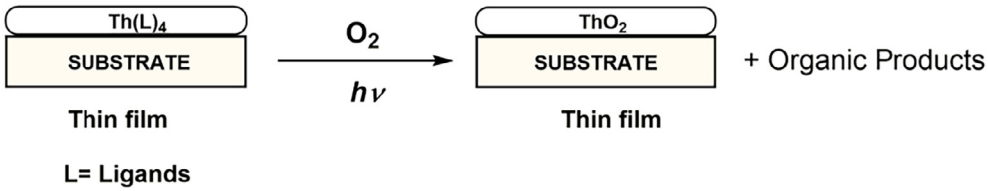

Scheme 1. Photodeposition of thorium oxide thin film.

a sensing property [29]. For this study, carbon monoxide gas was selected as a probe gas.

2. Experimental section

2.1. Materials

All solvents were of analytical grade and used directly (Merck). Acetylacetone (acac) and $Th(NO_3)_4xH_2O$ were obtained from Aldrich and used without further purification.

2.2. Syntheses of the tetrakis acetylacetonate thorium (IV) complex

$Th(acac)_4$ was synthesized according to the following general method [30].

Acetylacetone (4 mol) in ethanol was added to $Th(NO_3)_4$ (1 mol) in water, followed by the addition of ammonia (6 N) drop by drop until the mixture became alkaline. The white precipitate of thorium acetylacetonate was removed by filtration, washed with distilled water until neutral and purified by high vacuum sublimation; yield 57%; m.p. (°C) 171–172; IR (KBr, cm^{-1}): 1582 (s, νC=O), 1522 (s, νC=C). ^1H NMR ($CDCl_3$, δ ppm): 1.94 (s, 6H, $2CH_3$), 5.45 (s, 1H, CH). ^{13}C NMR ($CDCl_3$, δ ppm): 27.3 (CH_3), 104.0 (CH), 190.6 (CO). Mass spectrum (*m/z*): 628 (12) [M^+], 529 (23) [M^+ - $C_5H_7O_2$], 429 (30) [M^+ - $2C_5H_7O_2$], 347 (100) [M^+ - 281]; UV–Vis (in EtOH) λ_{max} (log ε): 287 (4.5).

2.3. Thin films deposition

The substrates for the deposition of films were fused quartz microslides (2 × 2 cm, 1.1 mm thickness) from Specialty Glass Products, Penn. and p-type silicon (100) wafers (1 × 1 cm) obtained from Wafer World, Florida, USA. Prior to use, the wafers were cleaned successively with ether, methylene chloride, ethanol, and aqueous HF (50:1) for 30 s and then with deionized water. The wafers were dried in an oven at 110 °C and stored in glass containers.

Thin films of the precursors were prepared according to the following procedure. A silicon chip was placed on a spin coater and rotated at a speed of 1500 RPM. A portion (145 μL) of a solution of the precursor complex in solvents, such as EtOH, CH_2Cl_2, or acetone, was dispensed onto the substrates and allowed to spread. The motor was then stopped after 30 s, and a thin film of the complex remained on the chip. The quality of the films was examined by optical microscopy (1000x magnification).

2.4. Photolysis of complexes as films on Si (1 0 0) surfaces

All photolysis experiments were performed following the same procedure. The FT-IR spectrum of the starting film was first obtained. The chip was then placed under a UVS-38 lamp setup equipped with two 254 nm 8 W tubes in an air atmosphere. The progress of the reactions was monitored by determining the FT-IR spectra at different time intervals following the decrease in the IR absorption of the complexes. After the FT-IR spectrum showed no evidence of the starting material, the chip was rinsed several times with acetone to remove any organic products remaining on the surface prior to analysis. Post-annealing of the films was carried out at 550, 750 and 950 °C for 3 h in a programmable Lindberg furnace and allowed to return to room temperature slowly.

2.5. Characterization techniques

FT-IR spectra were obtained at a 2 cm^{-1} resolution in a Perkin–Elmer Model Spectrum One FT-IR spectrophotometer. UV spectra were obtained on a Hewlett–Packard 8452-A diode array spectrophotometer. The ^1H and ^{13}C NMR spectra were measured in a $CDCl_3$ or DMSO-d_6 solution on a Bruker Fourier 300 spectrometer. Atomic force microscopy (AFM) was performed with a Nanoscope IV Dimension 3100 (Digital Instruments) in tapping mode. X-ray photoelectron spectra (XPS) were recorded on an XPS-Auger Perkin–Elmer electron spectrometer Model PHI 1257, which included an ultra high vacuum chamber, hemispherical electron energy analyzer and X-ray source providing unfiltered Kα radiation from its Al anode (hν = 1486.6 eV). The pressure of the main spectrometer chamber during data acquisition was maintained at 10^{-7} P. X-ray diffraction patterns were obtained using a Rigaku Dmax-2100 X-ray diffractometer. The X-ray source was Cu (Kα1 = 1.5406 Å) 30 kV/20 mA (600 W). The geometric configuration was a parallel beam with an angle of incidence of 1°. The scanning range was 25–80° of 2θ. The film thickness was determined using variable angle spectroscopic ellipsometry (SE) measurements in the spectral range of 1.5–5.0 eV. SE measurements were performed at incidence angles of 65° and 70° with a phase modulated ellipsometer (Jobin Yvon Uvisel DH10). The data were modeled using Film Wizard software. Photoluminescence (excitation-emission) spectra of films were obtained on a Jasco FP-8200 spectrofluorimeter at room temperature. The excitation wavelength was 366 nm, and the emission spectra were measured between 400 and 720 nm. Evaluation of the PL sensing capacity was carried out in a multifrequential spectrofluorimeter of phase and modulation ISS model K2. A KV 399 nm cut-off filter was used. Emission and excitation sweeps were performed between 390 and 720 nm and 390–450 nm, respectively. The CO concentration used was 62.26 ppm. All spectra were determined at room temperature.

3. Results and discussion

3.1. Photochemistry of the $Th(acac)_4$ complex

Although the photochemical properties of many 1,3-diketonate metal complexes have been extensively studied [31], no reports can be found in the literature regarding the photochemistry of thorium complexes with diketonate ligands. We therefore carried out experiments to evaluate the photosensitivity of the $Th(acac)_4$ complex in solution and as films. The electronic spectrum of the complex in EtOH shows absorption at λ_{max} = 298 nm (log ε = 4.2). Since Th(IV) does not participate in low-energy electronics transition, charge transfer (CT) and metal-centered (MC) excited states do

not exist; therefore, the absorption observed in the UV spectrum of $Th(acac)_4$ can only be assigned to an intraligand (IL) band. When ethanol solutions of $Th(acac)_4$ were irradiated with 300 nm UV light, a rapid decrease in the absorption bands was observed after 34 min of irradiation. Fig. 1a shows the UV profile of the photoreaction obtained by determining the UV spectra of samples taken at different time intervals. These results demonstrated that the Th(IV) complex was highly photoreactive in solution when irradiated with 300 nm UV light.

To investigate the solid-state photochemistry, a film of Th(IV) acetylacetonate was deposited on Si wafers by spin-coating and irradiated under an air atmosphere with a 254 nm UV lamp. FT-IR was used to monitor the photochemical reaction. FT-IR spectra of the film were collected at various exposure times. Fig. 2 shows the FT-IR spectra obtained in the range of 500–1700 cm^{-1}. All of the absorptions associated with the acetylacetonate ligand disappeared after 50 min of UV exposure, indicating the decomposition of the precursor and loss of organic groups in the film upon UV irradiation.

3.2. Characterization of ThO_2 thin films (XRD and XPS)

The elemental compositions of as-deposited and annealed UV-irradiated films were analyzed by XPS to investigate the chemical nature of the deposited surface. Fig. 3 shows the wide scan XPS spectrum over a binding energy range of 0–1000 eV of a UV-irradiated thin film photodeposited on a Si(100) surface. As expected, only Th, O and C contributions were observed in the spectrum. The C1s peak observed at 284.9 eV in the as-deposited film was probably the result of surface contamination rather than inefficient photolysis, which was confirmed by the sharp decrease observed in the carbon signal after annealing at 550 °C.

The binding energy values of Th $4f_{5/2}$, $4f_{7/2}$ signals and O 1 s signal of the as-deposited and annealed ThO_2 thin films show slight differences that evidences the partial formation of oxidation of thorium oxide (ThO_{2-X}) and the stoichiometric oxidation (ThO_2) for the as-deposited and annealed samples, respectively [15,32].

For annealed samples, the photoelectronic lines of $4f_{5/2}$ y $4f_{7/2}$ for thorium consist of two perfect Gaussian peaks located at 343.7 and 334.4 eV, respectively (Fig. 4a). These peaks are due to the spin–orbit Th 4f levels corresponding to $4f_{5/2}$ and $4f_{7/2}$, in which

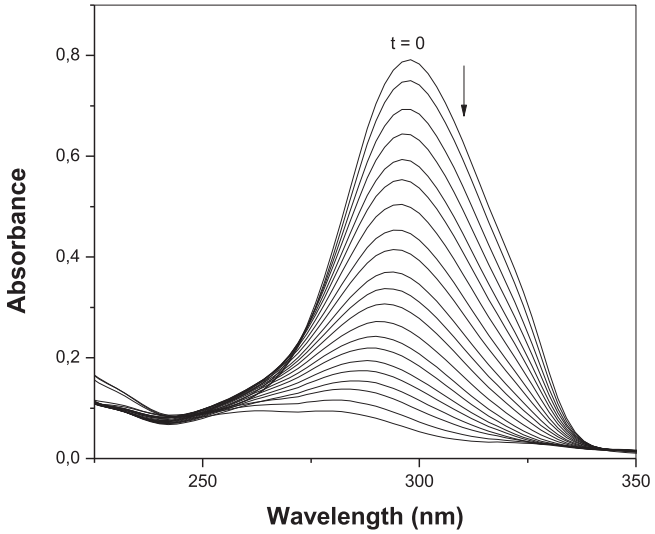

Fig. 1. Changes in the UV spectrum (2 min intervals) of a solution of the Th(IV) acetylacetonate complex (5.2×10^{-5} M in EtOH) upon 34 min of irradiation with 300 nm light.

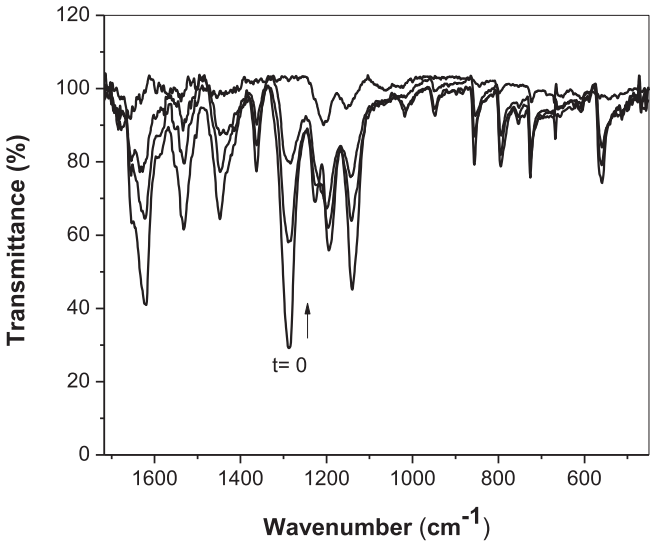

Fig. 2. Changes in the FT-IR spectrum of a film of bis(2,4-pentanedionato)Thorium (IV) (300 nm thickness) deposited on Si(100) exposed to 254 nm light for 0, 10, 30 and 50 min.

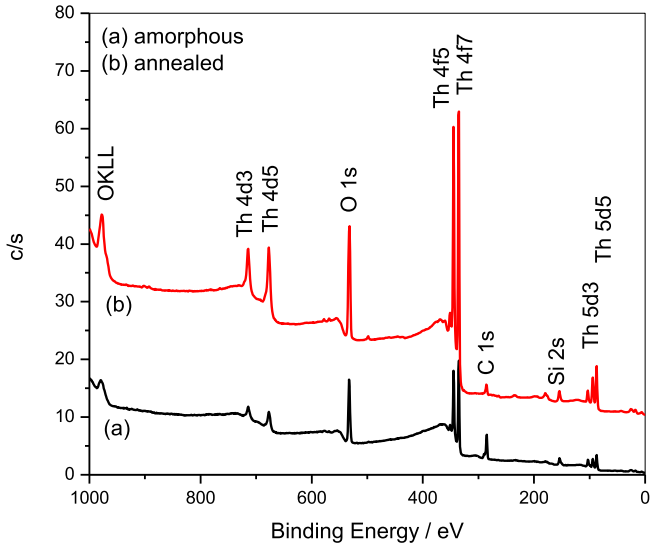

Fig. 3. Wide-scan XPS spectrum of a photodeposited ThO_2 film on Si(100) (a) as-deposited or (b) annealed under an air atmosphere at 550 °C for 3 h.

the 4f doublet lines are separated by 9.3 eV. These peaks and a small satellite at 6.51 eV in front of the Th $4f_{5/2}$ peak agreed with those observed by Dash et al. [33]. The peak positions and energy separations are in good agreement with data reported for ThO_2 films [32–36] and conclusively establish that, in crystalline films, Th is only present in the Th^{+4} state.

The photoelectronic high resolution O1s line showed two peaks (Fig. 4b). The first component located at lower energy (530.4 eV) can be assigned to oxygen atoms that strongly bonded to the metal (M–O), and the second O1s peak, located at higher energy (531.7 eV), corresponds to oxygen in water molecules that bound to the film structure or adsorbed on the sample surface.

This result infers that a film of Th(IV)acetylacetonate can be converted to a ThO_2 film by UV irradiation at room temperature with post-annealing.

XRD characterization revealed the amorphous nature of the as-deposited films since no diffraction peaks could be observed

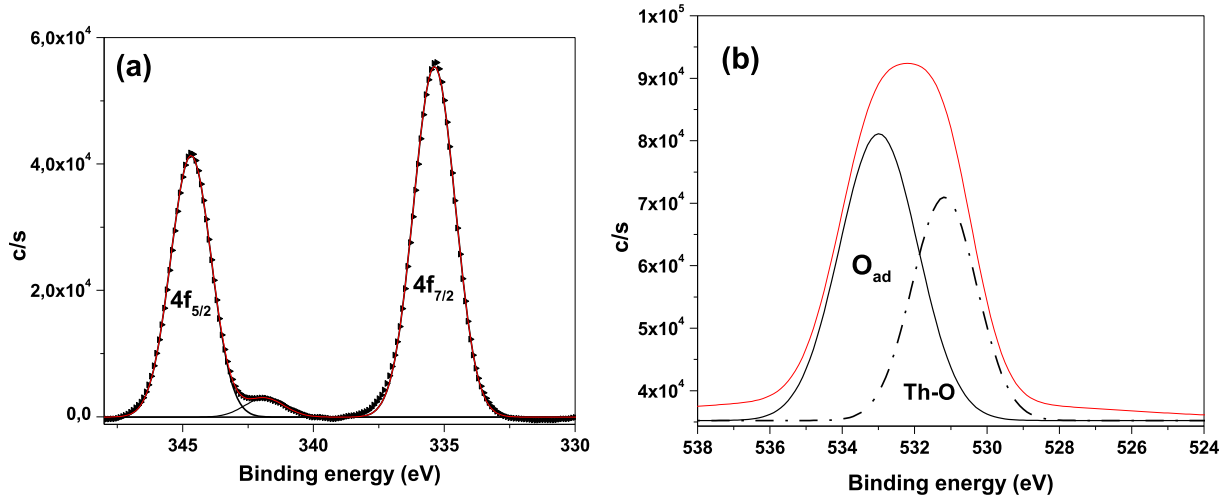

Fig. 4. Narrow scan XPS spectrum of a photodeposited ThO_2 film annealed at 550 °C: (a) Th $4f_{5/2}$ and $4f_{7/2}$ lines, and (b) O1 s lines.

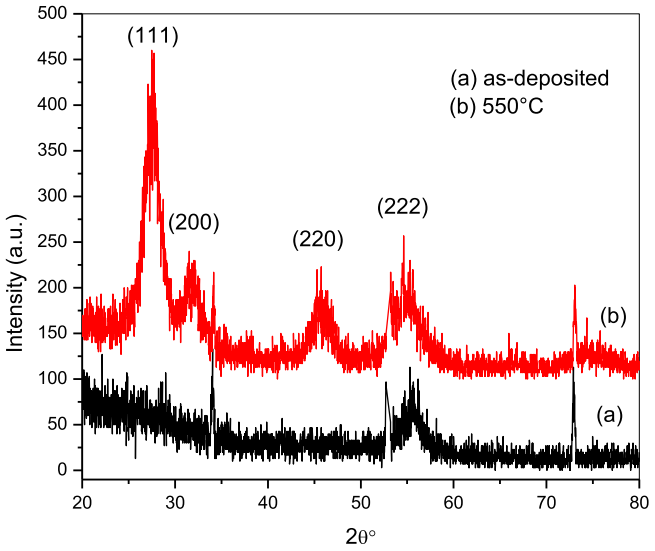

Fig. 5. XRD diffractogram of a ThO_2 thin film (a) as-deposited and (b) annealed for 3 h at 550 °C.

(Fig. 5). However, the XRD spectra of films annealed at 550 °C showed a well-developed crystalline structure with reflections that could be assigned to crystalline cubic ThO_2 (Fig. 5). The spectrum of the annealed films showed ThO_2 lines at $2\theta = 27.6°$, 31.9°, 45.8°, 54.3° and 56.9° corresponding to the (111), (200), (220), (311) and (222) planes of crystalline ThO_2, respectively, in a cubic geometry with a space group Fm-3m (JCPDS 4-0556) [34]. This result indicates that films have a strong (111) preferred orientation. The broadening of the XRD peaks of this sample suggests that its crystallite size is very small. Using the well-known Scherrer's equation [35] based on the half-width of the (111) peak in its XRD pattern (Fig. 5), the crystallite size of the ThO_2 film annealed at 550 °C was estimated to be 2.9 nm. As the annealing temperature was increased, the average crystallite size of the samples also increased, as shown in Table 1. The XRD data confirmed a preferred (111) orientation for the ThO_2 fluorite crystallites which is in good agreement with previous work on thin ThO_2 films grown on polycrystalline Ir by PVD [13].

3.3. Morphological analysis of ThO_2 thin films (AFM)

Fig. 6 shows the surface topography of as-deposited and annealed ThO_2 films deposited on Si(100) substrates recorded by atomic force microscopy. The AFM image of an as-deposited ThO_2 thin film (Fig. 6a) shows a non-uniform rough surface with a root-mean-square (rms) roughness of 7.14 nm. This surface can be described as fibrous without structural order, which is characteristic of an amorphous deposit. On the other hand, after heating at 550 °C for 4 h in air, the ThO_2 film showed a more uniform and smoother surface with a rms roughness of 3.34 nm (Fig. 6b). The thickness of the as-deposited and annealed films was determined by variable angle spectroscopic ellipsometry. The results show that the thickness of a $Th(acac)_4$ precursor film decreases after photolysis from 300 nm to 85 nm for the as-deposited ThO_2 film, which is less than 1/3 of its original value.

As shown in Table 1, as the annealing temperature increased (>550 °C), the thickness and roughness of the films also increased. The results showed that the surface roughness increased from *Rs* = 3.34 to 9.17 to 11.52 nm with increasing film thickness from 29.4 to 40.2 to 107 nm, respectively.

3.4. Optical characterization of ThO_2 films

The optical transmission spectra of the as-deposited and annealed films over the wavelength range of 220–900 nm are shown in Fig. 7. The transmission spectra of these films show an optical transmittance in the visible region above 95% for as-deposited films and 85% for annealed films. This decrease in the level of transparency is due to the fact that the thermal treatment decreases the thickness of the film and contributes to granting a greater compactness of the deposit when compared with the as-deposited films. The intense absorption at ~240 nm of annealed samples can be attributed to the top of the upper valence band with a potential dominant contribution from the partial hybridization between the Th6d and O2p states or ascribed to the charge-transfer transitions from oxygen to the thorium [36].

From the solid band theory, the relation between the absorption coefficient and energy of the incident light $h\nu$ is given by the Tauc equation [37,38]:

$$\alpha h\nu = A(h\nu - E_g)^n$$

where A is the probability parameter for the transition, α is the absorption coefficient of the material, $h\nu$ is the photon energy, E_g

Table 1
Values of thickness, grain size, surface roughness, band gap energy and sensing efficiency of ThO_2 films annealed at different temperatures (T).

Annealing T (°C)	Thickness (nm)	Grain size (nm)	Roughness (Rms) (nm)	Band Gap (eV)	Sensing efficiency (%)
As-deposited	85		7.14	4.50	22
550	29.4	2.9	3.34	4.61	36
750	40.2	3.8	9.17	4.54	15
950	107	8.8	11.52	4.50	10

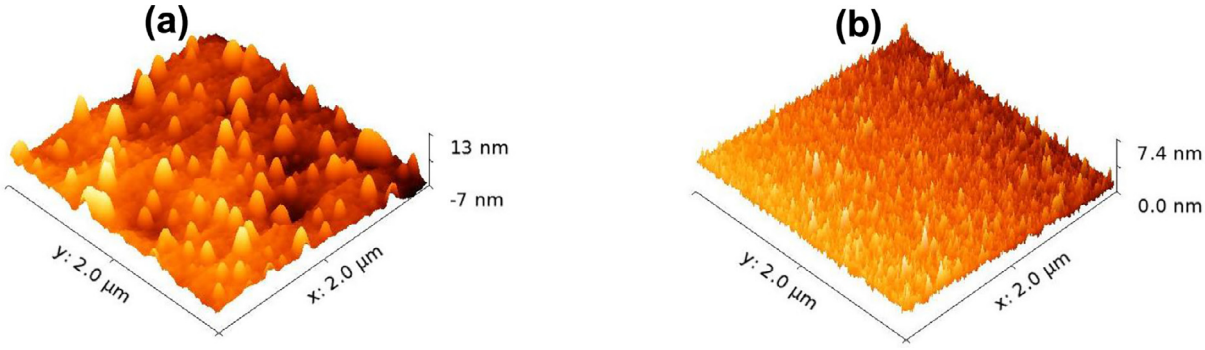

Fig. 6. AFM micrography of a ThO_2 thin film on Si(100) (a) without thermal treatment and (b) annealed at 550 °C (image size 2 × 2 µm).

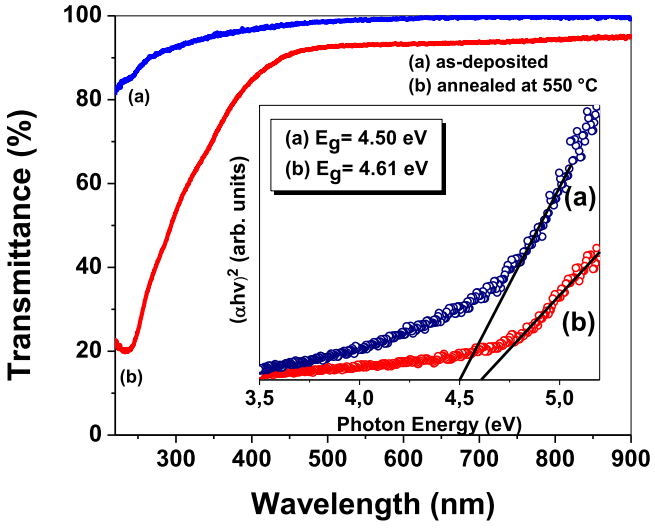

Fig. 7. Effect of the annealing temperature on the optical transmission of ThO_2 thin films; inset: Tauc's plot $(\alpha h\nu)^2$ versus photon energy for ThO_2 thin films as-deposited and annealed at 550 °C.

is the optical band gap energy and n determines the type of electronic transition caused by the absorption and can have values of 1/2 for transitions in amorphous materials or 2 for transitions in crystalline materials [39,40]. Table 1 summarizes the optical band gaps of ThO_2 thin films annealed at different temperatures.

As-deposited thin films have a band gap energy of 4.5 eV, and films treated at 550, 750 and 950 °C have band gaps of 4.61, 4.54 and 4.50 eV, respectively. This behavior is directly related to the grain size. As shown in Table 1, at higher temperatures, the grain size increased, which led to a decrease in the optical band gap. The reduction in band gap reflected the creation of intermediate levels between the valence and conduction bands of thoria [40], as well as due to the creation of point defects such as oxygen vacancies in this structure [41]. Diverse theoretical studies have determined the ThO_2 band gap in a wide range from 4.4 to 6.9 eV [42] and experimental works suggest that the band gap is between 3.8 [12] and 5.9 eV [43]. In a recent work, Pereira et al. [36] determined a value of 5.4 eV for the direct band gap energy of pure thoria nanoparticles with an average crystallite size of 10 nm. Although this value of Eg agrees well with the experimental band gap energy reported for single-crystal ThO_2 (5.8 eV), the reported data from theoretical as well as experimental studies shows that the optical band gap energy is very sensitive to the preparation method and the experimental parameters applied in the synthesis [43]. Theoretical studies [44] have revealed that the generation of point defects in ThO_2 creates a charged system and defects can cause very long-range structural perturbations.

In this work, it is observed for annealed samples, that with an increase in the calcination temperature, the morphology characteristics such as thickness, grain size and roughness of the films gradually increase and consequently the number of intrinsic defects in the material also increases contributing to the reduction of band gap values.

3.5. Luminescent properties of ThO_2 thin films

The inset of Fig. 8 shows the excitation spectra, which reveal one broad band at 366 nm by monitoring with emission wavelength at 697 nm. The position of the band at 366 nm is attributed to absorption of charge transfer $Th^{IV}/Th^{III} \leftrightarrow Th^{III}/Th^{IV}$ under non-stoichiometric conditions (ThO_{2-x}) [36].

The PL spectra of the as-prepared and annealed ThO_2 thin films with an excitation wavelength of 366 nm are shown in Fig. 8. The PL spectra exhibit two types of emission, one of them, a blue emission with a band centered at 400 nm with a small shoulder at 419 nm, and the other red emission that has been observed at 686 and 707 nm. The blue emission is attributed to radiative recombination involving defect sites at the surface of ThO_2 films and has been observed by other authors [45–47]. Probably these bands are due to oxygen vacancies that induce the donor levels and the recombination of an electron on a donor with a hole on an acceptor formed by a thorium vacancy or a thorium-oxygen vacancy pair, phenomenon very similar to what happens in many metallic oxides. On the other hand, the red emission could be associated with defects or vacancies in the oxide network due to intermediate energy levels in the band gap [48].

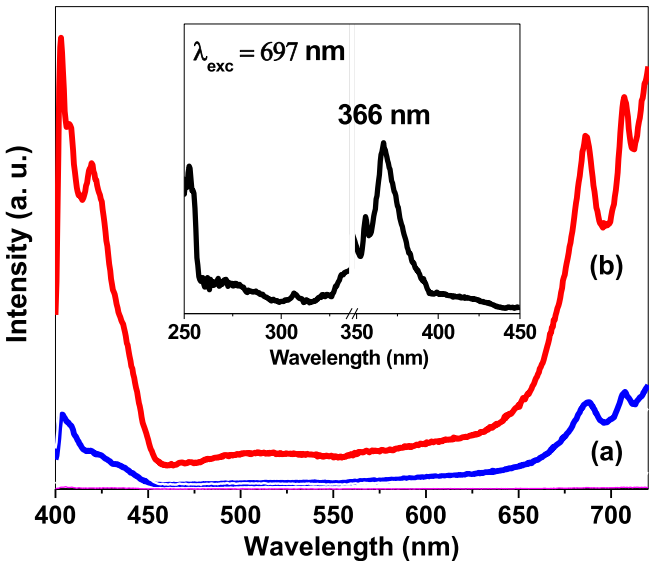

Fig. 8. Room temperature PL spectra of a ThO_2 thin film (a) as-deposited (blue) and (b) annealed at 550 °C (red) (excitation at 366 nm). Inset: room temperature excitation spectrum at 697 nm laser line. (Colour online.)

3.6. Sensing properties of ThO_2 thin films

To evaluate the luminescent sensing capacity of ThO_2 thin films, we measured the quenching of the PL emission of annealed thin films when exposed to carbon monoxide gas (CO) at a concentration of 60 ppm/N_2 at room temperature. During sample exposure to CO gas, the only significant effect in the emission spectrum was a reduction of the PL intensity, while no shift of the emission peak or change in its line shape was observed. (Fig. 9). The parameters considered to evaluate their behavior as sensors were the response time and recovery time. The response time was less than 30 s, while the recovery time was much longer. PL-based sensors usually have the advantage of working at low temperatures, but we observed that, in our case, high temperatures were required to promote the desorption of strongly bonded species, thus partially reducing this advantage. Sensor recovery was 90% after subjecting the films to 120 ° C for 3 h.

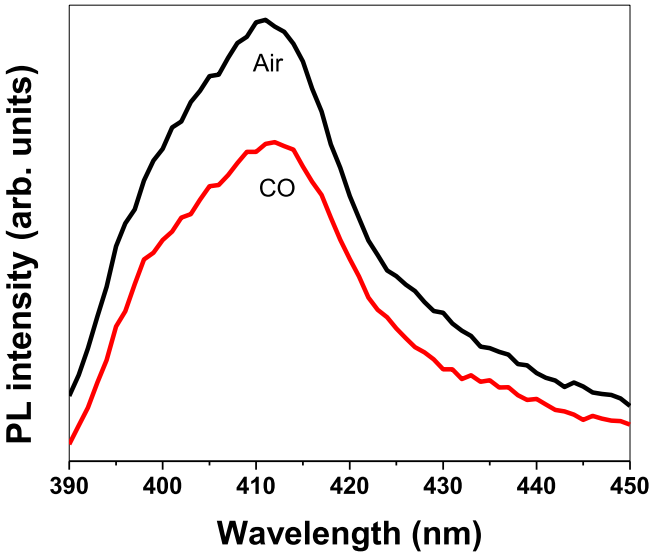

Fig. 9. PL spectra at room temperature for a ThO_2 film (annealed at 550 °C). Black line: sample in synthetic air. Red line: sample in 60 ppm of CO gas.

The quenching efficiency is given by the expression 1- (A/A_0) × 100, where A/A_0 is the ratio of areas under standardized PL curves for a sensor without a quencher (A_0) and with a quencher (A). As shown in Table 1, the highest quenching efficiency (36%) was obtained with ThO_2 films annealed at 550 °C with an average grain size of 2.9 nm, probably due to the high surface-volume ratio. As expected, the larger the grain size, the lower the sensor sensitivity.

This decrease of the PL intensity may be related to the interaction between the CO molecules and ThO_2 surface. The chemical reactions occurring at the oxide surface are assumed to involve CO adsorption, desorption of CO_2 and replenishment of the resulting surface oxygen vacancy by the adsorption of molecular oxygen [49]. When the sensor is exposed to CO gas, different reactions can take place with the surface chemisorbed oxygen. These reactions of CO adsorbed over the surface introduce non-radiative recombination paths that modify the emission processes of the thin films.

4. Conclusion

The results of this study demonstrate that a Th(IV)acetylacetonate film can be converted to a ThO_2 film by UV irradiation at room temperature. Photodeposition of the ThO_2 thin film on a Si(100) wafer at room temperature produces, after annealing at 550 °C and above, a polycrystalline film that has a preferential orientation along the ThO_2 (111) direction, as demonstrated by X-ray diffraction. The gas sensitivity results showed that ThO_2 films annealed at 550 °C were very sensitive to CO gas. The PL spectrum of a ThO_2 thin film was reversibly quenched by the introduction of 60 ppm of CO at room temperature. Although these results are promising in terms of thorium oxide thin films being used as luminescent gas sensors, further gas-sensing parameters still need to be evaluated, such as, its selectivity to reducing gases, as well as its long-term stability.

Acknowledgments

G.B.C. acknowledges FONDEQUIP (EQM 130154). Y.H. thanks CONICYT (CHILE) for the doctoral fellowship (N° 21110277).

References

[1] G. Adachi, N. Imanaka, S. Tamura, Chem. Rev. 102 (2002) 2405.
[2] T. Griffiths, J. Dixon, Inorg. Chim. Acta 300 (2000) 305.
[3] P. Harvey, J. Hallett, J. Solid State Chem. 12 (1975) 219.
[4] R. Bressat, M. Breysse, B. Claudel, H. Sautereau, R. Williams, J. Lumin. 10 (1975) 171.
[5] R. Bressat, B. Claudel, J. Puaux, R. Williams, M. Breysse, L. Faure, J. Catal. 40 (1975) 286.
[6] M. Breysse, B. Claudel, L. Faure, M. Guenin, R. Williams, T. Wolkenstein, J. Catal. 45 (1976) 137.
[7] M. Breysse, B. Claudel, M. Guenin, L. Faure, Chem. Phys. Lett. 30 (1975) 149.
[8] W. Evans, D. Allred, Thin Solid Films 515 (2006) 847.
[9] Jed E. Johnson, David D. Allred, R. Steven Turley, William R. Evans, and Richard L. Sandberg, in Actinides—Basic Science, Applications, and Technology, 893 (Material Research Society Symposium Proceedings, 2005)
[10] Nicole F. Brimhall, R. Amy Baker, Steven Turley, David D. Allred, 6317–36, in Advances In X-Ray/EUV Optics, Components, And Applications, 2006.
[11] R. Niranjan, K. Patil, S. Sainkar, K. Vijayamohanan, I. Mulla, Mater. Chem. Phys. 84 (2004) 37.
[12] S. Mahmoud, Solid State Sci. 4 (2002) 221.
[13] M. Bagge-Hansen, R. Outlaw, K. Seo, D. Manos, Thin Solid Films 520 (2012) 4249.
[14] R. Reibold, J. Poco, T. Baumann, R. Simpson, J. Satcher, J. Non-Cryst. Solids 341 (2004) 35.
[15] P. Cakir, R. Eloirdi, F. Huber, R.J.M. Konings, T. Gouder, J. Phys. Chem. C 118 (2014) 24497.
[16] J. Rangel Costa, G. Marchetti, M. Rangel, Catal. Today 77 (2002) 205.
[17] R. Niranjana, M. Londheb, A. Mandalea, S. Sainkara, L. Prabhumirashib, K. Vijayamohanana, I. Mulla, Sens. Actuators B87 (2002) 406.
[18] F. Wang, F. Zhu Ge, H. Zhang, B. Ding, Mater. Res. Bull. 38 (2003) 629.

[19] F. Zhuge, Z. Ye, F. Wang, Y. Wang, H. Zhang, B. Ding, Mater. Lett. 57 (2003) 2776.
[20] N. Clavier, J. Maynadie, A. Mesbah, J. Hidalgo, R. Lauwerier, G.I. Nkou Bouala, S. Parres-Maynadi, D. Meyer, N. Dacheux, R. Podor, J. Nucl. Mater. 487 (2017) 331.
[21] Tereza Pavelková, Václav Cuba, Ferdinand Šebesta, J. Nucl. Mater. 442 (2013) 29.
[22] G. Cabello, L. Lillo, Y. Huentupil, F. Cabrera, G.E. Buono-Core, B. Chornick, J. Phys. Chem. Solids 72 (2011) 1170.
[23] G.E. Buono-Core, M. Tejos, H. Klahn, G. Cabello, A. Lucero, R. Hill, J. Chil. Chem. Soc. 52 (2007) 1218.
[24] G. Cabello, L. Lillo, G.E. Buono-Core, J. Non-Cryst. Solids 354 (2008) 982.
[25] G. Cabello, L. Lillo, C. Caro, G.E. Buono-Core, B. Chornik, M. Soto, J. Non-Cryst. Solids 354 (2008) 3919.
[26] G.E. Buono-Core, H. Klahn, M. Tejos, R. Hill, Bol. Soc. Chil. Quim. 43 (1998) 339.
[27] G.E. Buono-Core, H. Klahn, C. Castillo, M. Bustamante, E. Muñoz, G. Cabello, B. Chornik, Polyhedron 30 (2011) 201.
[28] G.E. Buono-Core, G. Cabello, A. Klahn, A. Lucero, M. Nuñez, B. Torrejón, C. Castillo, Polyhedron 29 (2010) 1551.
[29] V.M. Zhyrovetsky, D.I. Popovych, S.S. Savka, A.S. Serednytski, Nanoscale Res. Lett. 12 (2017) 132.
[30] W. Fernelius, Inorganic Syntheses, McGraw-Hill, 1946, p. 123, Vol. II.
[31] B. Marciniak, G.E. Buono-Core, J. Photochem. Photobiol., A: Chem. 52 (1) (1990) 1.
[32] Y.A. Teterin, A.Y. Teterin, N. Yakovlev, I. Utkin, K. Ivanov, L. Shustov, L. Vukcevic, G. Bek-Uzarov, Nucl. Technol. Radiat. 2 (2003) 31.
[33] S. Dash, A. Singh, P. Ajikumar, H. Subramanian, M. Rajalakshmi, A. Tyagi, A. Arora, S. Narasimhan, B. Raj, J. Nucl. Mater. 303 (2002) 156.
[34] S. Gupta, R. Gupta, V. Natarajan, S. Godbole, Mater. Res. Bull. 49 (2014) 297.
[35] B.D. Cullity, In Elements of X-Ray Diffraction, Addison-Wesley, Reading, MA, 1956, p. 99.
[36] F.J. Pereira, M.A. Castro, M.D. Vázquez, L. Debán, A.J. Aller, J. Lumin. 184 (2017) 169.
[37] J. Tauc, R. Grigorovici, A. Vancu, Phys. Stat. Sol. 15 (1966) 627.
[38] J. Tauc (Ed.), Amorphous and Liquid Semiconductor, Plenum Press, New York, 1974.
[39] J. Cisneros, Appl. Optics 37 (1998) 5262.
[40] Jyoti Pandey, Aanchal Sethi, Sitharaman Uma, Rajamani Nagarajan, ACS Omega 3 (2018) 7171.
[41] Promila Kumari, Meenakshi Pokhriyal, Sitharaman Uma, Rajamani Nagarajan, ChemistrySelect 3 (3) (2018) 5005.
[42] T.D. Kelly, J.C. Petrosky, D. Turner, J.W. McClory, J.M. Mann, J.W. Kolis, Xin Zhang, P.A. Dowben,, Phys. Status Solidi RRL 8 (3) (2014) 283.
[43] W.R. Evans, D.D. Allred, in: Ali M. Khounsary, Christian Morawe, (eds.) Advances In X-Ray/EUV Optics, Components, and Applications, 6317, Proceedings of SPIE, (2006).
[44] Rakesh K. Behera, Chaitanya S. Deo, J. Phys. Condens. Matter 24 (2012) 215405.
[45] M. Breysse, B. Claudel, L. Faure, M. Guenin, J. Colloid Interf. Sci. 70 (1979) 201.
[46] M. Breysse, B. Claudel, L. Faure, M. Guenin, J. Lumin. 18 (1979) 402.
[47] Z. Lin, Q. Kuang, W. Lian, Z. Jiang, Z. Xie, R. Huang, L. Zheng, J. Phys. Chem. B 110 (2006) 23007.
[48] Vikash Kumar Tripathi, Rajamani Nagarajan, Inorg. Chem. 55 (2016) 12798.
[49] J.F. McAleer, P.T. Moseley, J.O.W. Norris, D.E. Williams, JCS Faraday I Trans. 83 (1987) 1323.